Dalton Transactions

ROYAL SOCIETY OF CHEMISTRY

PAPER

View Article Online
View Journal

Cite this: DOI: 10.1039/d2dt00950a

Highly emissive supramolecular gold(I)–BTD materials†

Andrea Pinto,[a,b] Marcelo Echeverri,[c] Berta Gómez-Lor *[c] and Laura Rodríguez *[a,b]

Herein we report the synthesis of three light emitting rod-shaped gold(I) complexes by combining ethynyl-functionalized 2,1,3-benzothiadiazole (BTD), with different N-heterocyclic (imidazole, benzimidazole and phenantroimidazole) carbene gold(I) complexes. As could be determined by single crystal structure determination, the size of the N-heterocyclic carbene affects the relative disposition of the two ligands in the linear gold complexes (nearly perpendicular in the benzimidazole *vs.* planar in the phenantroimidazole derivative) which translates to different types of interactions between neighbouring units. In fact, the planar conformation in the more π-extended phenantroimidazole carbene allows Au(I) atoms to get sufficiently closer favouring aurophilic interactions. This compound is obtained as two different colour emitting solids which is ascribed to changes in packing modes probably leading to differences in the strength of aurophilic interactions. Interestingly, while the emission in the solid state is almost quenched, the incorporation of the compounds in polymer matrixes enhances the emissive properties of the compounds reaching near unity quantum yields.

Received 28th March 2022,
Accepted 27th April 2022

DOI: 10.1039/d2dt00950a

rsc.li/dalton

Introduction

There is rapidly growing interest in the last years in the development of metal-acetylide (π) organometallic systems for smart applications in optoelectronics such as flexible organic photovoltaics (OPV), organic light emitting diodes (OLED), and field effect transistors (FET).[1–5] Special attention is being focused on developing organic light-emitting materials for OLED applications.[6–8] Many blue, green and red light emitting organic and organometallic conjugates have been developed,[6] but obtaining highly efficient emissive materials suitable to present 100% emission is still a challenge.

Controlling the light emitting properties of organic and organometallic solids is a difficult task, as they are not only governed by those of individual molecules but also depend on how they interact with their neighbouring units and therefore on how they are spatially ordered in the bulk. This high dependence of the final properties of the materials from the organization of the molecular units, however, offers many opportunities to obtain materials with light emitting properties tuneable by varying their supramolecular arrangement[9] and stimuli-responsive fluorophores.

Thus, supramolecular materials able to self-organize through the cooperation of different inter- and intramolecular contacts are interesting candidates in the search for molecular systems for optoelectronic applications[10,11] Suitable candidates should consist of organic moieties presenting both highly efficient light emitting properties and a strong propensity to self-aggregate. 2,1,3-Benzothiadiazoles (BTDs) appear as good candidates as this electron-deficient heterocycle presents high fluorescence quantum efficiencies both in solution and in the solid state. On the other hand, the flat topology of this moiety together with the presence of chalcogen and nitrogen atoms in its structure confers this moiety a strong tendency to establish cooperative intermolecular interactions such as chalcogen bonding and π–π stacking. Thanks to their impressive optical properties BTD derivatives have been widely used as components in the fabrication of organic light-emitting diodes (OLEDs),[12] organic solar cells (OSCs),[13] bioimaging,[14] fluorescence sensing,[15] and stimuli-responsive fluorophores,[16,17] and fluorescent lysosome-staining agents[18] among others.

Apart from the organic counterpart, the presence of specific metals able to perform M···M interactions appears as a good choice not only to modulate the resulting luminescence properties but also to improve and/or modulate the resulting supramolecular networks. In this context, gold(I) is one of the

[a]Departament de Química Inorgànica i Orgànica, Secció de Química Inorgànica, Universitat de Barcelona, Martí i Franquès 1-11, E-08028 Barcelona, Spain. E-mail: laura.rodriguez@qi.ub.es
[b]Institut de Nanociència i Nanotecnologia (IN²UB), Universitat de Barcelona, 08028 Barcelona, Spain
[c]Instituto de Ciencia de Materiales de Madrid, CSIC Cantoblanco, 28049 Madrid, Spain. E-mail: bgl@icmm.csic.es

†Electronic supplementary information (ESI) available. CCDC 2160186 and 2160187. For ESI and crystallographic data in CIF or other electronic format see DOI: https://doi.org/10.1039/d2dt00950a

most explored metal, leading to strongly luminescent materials. Aurophilic Au···Au interactions have been found to play a key role in tuning the electronic and luminescence properties and the supramolecular organization of a wide range of molecular structures.[1,19–24] and provide attractive design motifs to obtain materials with switchable luminescence in response to external stimuli, such as mechanical stress,[25] heat,[26] and solvent vapors.[27]

Luminescent 2,1,3-benzothiadiazole (BTD) derivatives and gold(I) complexes have been reported separately but gold(I)–BTD systems have been scarcely explored. In this work, we are focused on the combination of these two moieties in one material. To that end, we have synthesized new gold(I) BTD complexes by the complexation of a rod-like BTD ligand endowed on one edge with an ethynyl group[28] that will be used to complex gold atoms and on the other edge a *p*-nonylphenyl moiety, a group that has been previously shown to induce the assembly of these molecules in layers. The study of their luminescence properties, their supramolecular assemblies and the effect of the environment and external stimuli on their emission is also being presented.

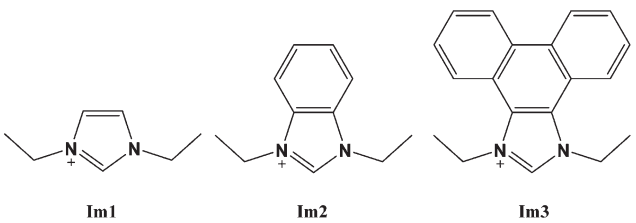

Fig. 1 Imidazolium salts used in this work.

Results and discussion

Synthesis and characterization

Synthesis of imidazolium salts. Three different imidazolium salts **Im1–Im3** that differ in their aromaticity of the backbones were synthesized (Fig. 1). **Im1** and **Im2** were synthesized by slight modifications of a previously reported experimental method (Scheme 1).[29,30] Briefly, commercially available imidazole and benzimidazole were reacted with ethyl iodide in acetonitrile yielding the imidazolium salts **Im1** and **Im2** in good yields. **Im3** was synthesized by slight modifications of a previously reported method that requires four different steps (Scheme 2).[31] The commercially available 9,10-phenanthrenequinone was initially reacted with formaldehyde and ammonium acetate in acetic acid to give 1*H*-phenanthro[9,10-*d*]imidazole. The subsequent deprotonation of the NH proton by the addition of a strong base yields the ionic compound that was isolated by the addition of diethyl ether. Then, the alkylation of the deprotonated imidazole with ethyl iodide at 130 °C in DMF yields 1-ethylphenanthro[9,10-*d*]imidazole. Finally, a second alkylation with ethyl iodide provides the imidazolium salt **Im3**.

Synthesis of gold(I) benzothiadiazole-based derivatives. Three different gold(I) benzothiadiazole derivatives were synthesized by a previously established method (Scheme 3)[32] by treating the imidazole salt with Ag_2O followed by a ligand exchange reaction with [AuCl(tht)]. Then, the labile chloride ligand was replaced by 4-ethynyl-7-(4-nonylphenyl)benzo[*c*][1,2,5]thiadiazole ligand (**L**)[28] previously deprotonated with KOH.

All complexes were characterized by ^{1}H NMR and IR spectroscopy as well as by ESI-MS (+) spectrometry (see the ESI†).

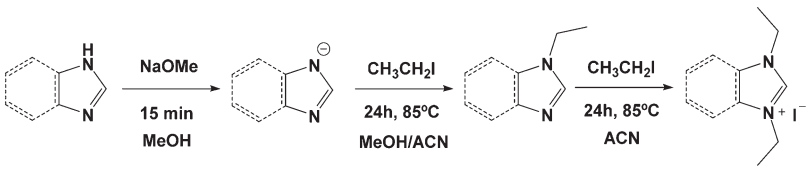

Scheme 1 Synthesis of the imidazolium salts **Im1** and **Im2**.

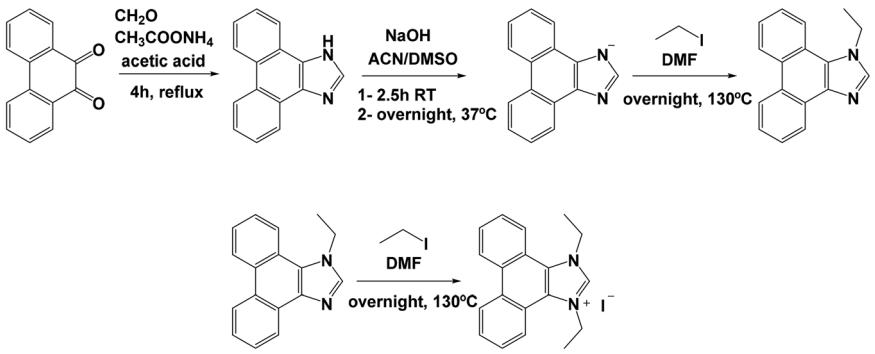

Scheme 2 Synthesis of the imidazolium salt **Im3**.

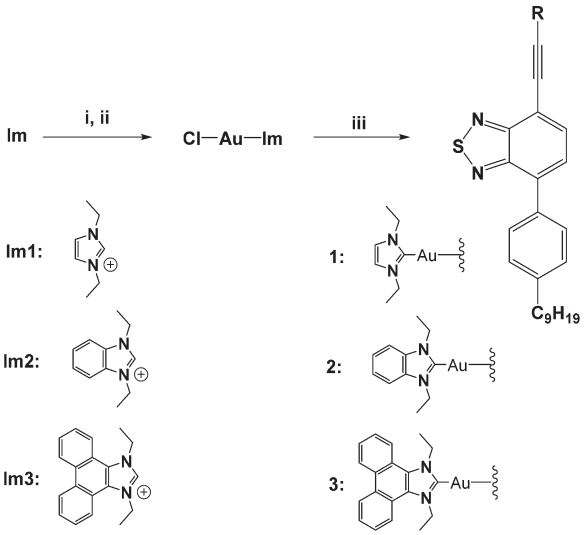

Scheme 3 Synthesis of gold(I) benzothiadiazole-based derivatives **1–3**. (i) Ag_2O in CH_2Cl_2, 40 °C, 6 h (for **Im1** and **Im2**), 72 h (for **Im3**); (ii) [AuCl(tht)], overnight, RT; (iii) **L** and KOH in MeOH/THF (1 : 2), overnight, RT.

The ^{1}H NMR spectra display the proton pattern of **L** as well as the protons related to the imidazole. Also, the disappearance of the N–C**H**–N proton of the imidazole part is a good indication of the successful coordination of the metal. The mass spectra show the monoprotonated species $[M + H]^+$ for **1–3**.

X-ray crystal structure determination

Single crystals suitable for X-ray diffraction of complexes **2** and **3** were grown from MeOH/THF/hexane solutions. They crystalize in the $P\bar{1}$ space group of the triclinic system. Selected bond length and angles are summarized in Table 1 and details of data collection and refinement are shown in Table S1.†

Compounds **2** and **3** both crystallize as a single molecule in the unit cell (Fig. 2). A linear geometry is observed for both complexes around the metal atom with C(Im)–Au–C angles of 176–178°. Bond distances between the gold(I) centre and the C of both ligands occupying the linear geometry and the imidazole and the alkynyl-BTD, are around 2.0 Å, similar to other compounds with an alkynyl and an imidazole attached to a gold(I) atom.[33,34] In both cases torsion angles around 20° between the BTD moiety and the linked phenylnonyl moieties are observed, however dihedral angles between the BTD and the imidazole ligands differ significantly in the two complexes being 67.28° to 8.40° in **2** and **3** respectively.

Table 1 Selected bond lengths (Å) and angles (deg.) for **2** and **3**

Compound	Distance (Å)	Angle (°)
2	Au–C(**Im2**): 2.009(4) Au–C: 1.979(4) Au···Au: 5.630(3)	C–Au–C: 176.06(1)
3	Au–C(**Im3**): 2.018(3) Au–C: 1.980(3) Au···Au: 3.360(4)	C–Au–C: 178.06(1)

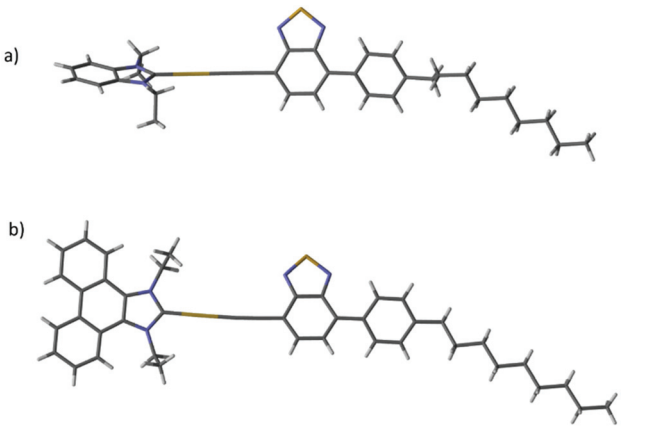

Fig. 2 Crystal structure of **2** (a) and **3** (b).

The packing of both compounds shows layered arrangements of the molecules that form dimeric species where the aliphatic chains point in an antiparallel manner (Fig. 2). In the case of **2**, these dimeric species are held by non-covalent interactions such as N–H···C_{sp}, C–H···π. In compound **3**, molecules form dimers through chalcogen-bonding 2S–2N squares, a common synthon in crystalline BTD derivatives.[35] These dimers interact with neighbouring dimers by π–π-stacking and aurophilic interactions (Au···Au of 3.36 Å) (Fig. S8 and S9†). The possibility of establishing aurophilic contacts in **3** is ascribed to the larger π-extended system of this compound, which lets the molecule stay in a planar disposition favouring Au···Au close contacts (Fig. 3).

Photophysical characterization

The absorption and emission spectra of all complexes **1–3** and the organic ligand **L** and **AuClIm** precursors were recorded in 10^{-5} M dichloromethane solutions and in the solid state at room temperature and the obtained data are summarized in Table 2 and shown in Fig. 4.

The absorption spectra of compounds **1–3** display three absorption bands. The two highest energy bands are related to the π–π* intraligand transition of the imidazole (Fig. 4 and S19, S20†)[36] and the benzothiadiazole and the lowest energy band is related to the charge transfer (CT) transition.[37–39] The charge transfer transition is *ca.* 40 nm red shifted in gold(I) complexes **1–3** with respect to **L**. This behaviour is probably due to an increase in the conjugation through mixing of the metal d-orbital with the π-system of the ligand.[40]

Emission spectra were recorded in solution and in the solid state upon excitation of the samples at the lowest energy absorption band (*ca.* 410 nm). Very weak emission was recorded for the **Im** and **AuClIm** precursors and thus, special attention has been paid to the emission properties of the final gold(I) complexes **1–3**. The emission of these complexes displays a structureless band around 500 nm that is *ca.* 30 nm red shifted with respect to **L** in solution (Fig. 4) and in all cases is completely dominated by the BTD chromophore while the

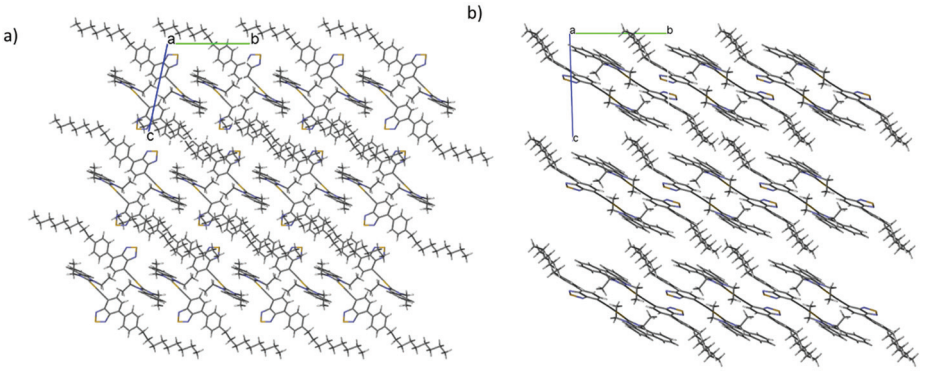

Fig. 3 View along *b* of the packing of **2** (a) and **3** (b).

Table 2 Electronic absorption and emission data, quantum yields (Φ_{fl}) and lifetimes (τ_{fl}) together with the calculated k_r and k_{nr} of **Im1–3**, **[AuCl(Im1–3)]**, **L** and pristine complexes **1–3**. Emission data, quantum yields, lifetimes, and k_r and k_{nr} in the solid state are displayed in bold

Compound	Absorption λ_{max} (ε, cm^{-1} M^{-1})	Emission	Φ_{fl}	τ_{fl} (ns)	k_r (ns^{-1})	k_{nr} (ns^{-1})
Im1	244 (14 000)	340	—	—	—	—
Im2	238 (19 500) 274 (8630)	355	—	—	—	—
Im3	257 (41 400) 286 (19 600)	360	—	—	—	—
[AuCl(Im1)]	241 (7853)	340	—	—	—	—
[AuCl(Im2)]	232 (23 500) 285 (13 870)	321	—	—	—	—
[AuCl(Im3)]	261 (47 080)	374, 430	—	—	—	—
L	270 (15 454) 384 (8007)	492/**485**	0.83/**0.36**	9.40/**5.8**	0.088/**0.062**	0.018/**0.11**
1	298 (13 000) 436 (5000)	531/**523**	0.88/**0.01**	10.2/**4.08**	0.086/**0.002**	0.012/**0.24**
2	243 (22 898) 297 (24 455) 412 (8232)	528/**528**	0.93/**0.03**	9.62/**3.59**	0.097/**0.007**	0.0073/**0.27**
3	257 (24 271) 298 (15 012) 419 (5265)	525/**515**	0.46/**0.03**	9.15/**4.18**	0.05/**0.007**	0.06/**0.23**

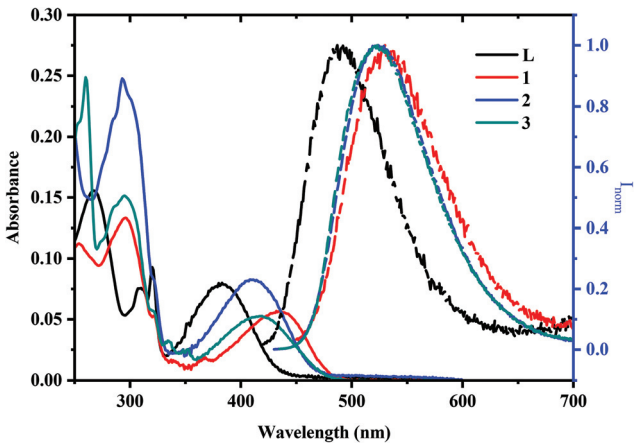

Fig. 4 Absorption (solid lines) and emission (dash lines) spectra of **L** and gold(I) complexes **1–3** in dichloromethane.

residual emission of the imidazole groups cannot be detected (see Fig. S19 and S20†). The observed large Stokes' shifts around 100 nm are a consequence of the efficient intramolecular charge transfer (ICT).[41] Excitation spectra collected at the emission maxima match the CT absorption bands at *ca.* 400 nm, as a direct indication of the origin of this emission. There is no significant change in the emission in solution and in the solid state for compounds **1** and **2**. In the case of compound **3**, a red shift in the emission in the solid state is observed (see Fig. S12†) probably due to the presence of aurophilic interactions in the solid packing.

Fluorescence quantum yields (Φ_{fl}) and lifetimes (τ_{fl}) were measured for those compounds that present high luminescence properties in dichloromethane and in the solid state (Table 2). In general, Φ_{fl} efficiencies recorded in solution are high with values above 80% in almost all cases, being above the values recorded for other BTD derivatives reported in the literature.[37–39,42,43] It can be observed that the presence of the Au-carbene increases the resulting quantum yields for **1** and **2**, being above 90% in **2**. In the case of **3**, which contains the imidazole ligand with the largest π-conjugation, the resulting quantum yield value is much smaller, around 50% (Table 2). This could be rationalized to the presence of aurophilic contacts that favour intersystem crossing and non-radiative triplet state population. The quantum yields recorded in the solid state are smaller, as previously observed in some BTD derivatives.[43,44] This decrease is more denoted in the presence of the gold(I) atom that may perform more efficient intermolecular packing favouring deactivation processes.

In all cases, the fluorescence lifetime profile shows a single-exponential decay, giving the τ_{fl} values in the range of 2–10 ns, which are in agreement with the assignment of a singlet state origin (fluorescence) and are in the high-range order than other BTD derivatives.[43,45,46] There is no significant change in these values when the gold is coordinated to the BTD struc-

ture, although they are slightly larger for **1** and **2** gold(I) complexes. Lifetimes are not so much affected by the packing (solid state) in contrast with quantum yields. Hence, the radiative (k_r) and non-radiative (k_{nr}) decay rate constants were calculated from the fluorescence quantum yields and lifetimes. The higher emission efficiency of **2** is also evidenced by the largest k_r and lowest k_{nr} calculated values. Additionally, k_{nr} governs the deactivation pathways in the solid state, explaining the significant decrease of quantum yields in this medium.

The mechanochromic properties of **L** and gold(I) complexes **1–3** were also investigated. Unfortunately, no significant changes could be observed upon grinding. However different emission colours could be observed for the as-obtained complex **3** (orange) or the single crystalline material (greenish) when visualized under a UV lamp (320 nm) even though both materials cannot be interconverted upon mechanical stress. Powder X-ray diffraction (PXRD) analysis shows that the pristine gold(I) complex **3** is obtained as a poorly crystalline solid (Fig. 5). The fact that both polymorphs cannot be interconverted upon mechanical stress points to a completely different crystal structure in the two differently emitting polymorphs. Crystal-to-crystal phase transitions require closely related initial and final phases as the mechanochromic transformation will involve changes of the supramolecular and/or intramolecular structure within the constrained environment of the crystal. The presence of stronger aurophilic interactions in the powder is probably the origin of the red-shifting observed in the emission. Generally speaking, the emission band is red shifted when aurophilic interactions are stronger due to the larger destabilization of the HOMO energy level of the gold complexes.

Hybrid materials

The compounds were dispersed in solid matrixes based on cellulose, polymethylmethacrylate (PMMA), polystyrene (PS) or the cyclic olefin copolymer, Zeonex, in order to favour the dispersion of the molecules avoiding close contact deactivation pathways observed in the solid state and increasing the quantum yield in the form of gold(I) highly luminescent materials. The corresponding emission spectra were recorded in all cases and a blue shift of the emission maxima (around 10 nm) with respect to the solid is observed when the compounds are introduced in the matrixes.

Quantum yields and lifetimes were measured in all cases and are summarized in Tables 3 and 4 and it can be observed that, in general trends, there is an increase of these properties when the compounds are introduced in the polymeric matrixes. In particular, the recorded quantum yields of **2** increase much more than the others. This could be ascribed to the non-planar conformation between the carbene and the BTD part of the molecule (see the above X-ray crystal structure) that precludes the intermolecular contacts. Thus, the inclusion of the compound in the matrix efficiently favors the radiative pathway (more rigid medium) but avoids the quenching for packing. It must be highlighted that the quantum yields and lifetimes are in the range of those previously recorded in solution and much larger than those obtained in the solid state. Emission efficiency close to 100% was obtained for **L** and **2** in PMMA, PS and Zeonex matrixes. These results are similar to those of the BTD derivatives containing phosphanes reported by us,[47] supporting the importance of the dispersion of the luminophores in organic materials to obtain highly luminescent materials.

Radiative and non-radiative constants have been calculated in order to rationalize the excellent recorded quantum yields (Table 5). In general, the introduction of the compounds in thin films decreases the non-radiative constants. The introduction of the compounds in matrixes enhances the luminescence properties and allows the dispersion of the molecules avoiding aggregation processes that quench the resulting emission observed in the solid state. Of note is the case of **3** that was substantially affected by the packing in the solid and presents

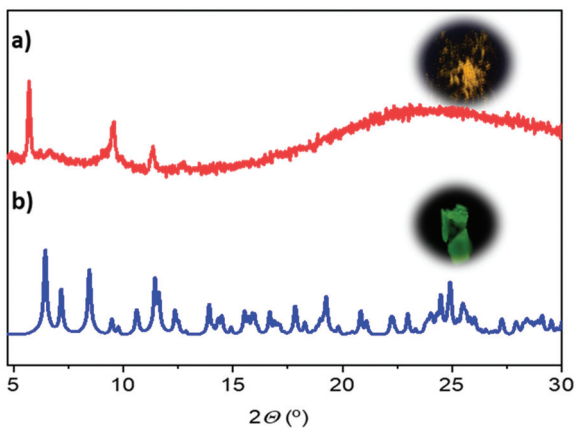

Fig. 5 (a) PXRD and photographs of as-obtained complex **3** (b) and single crystalline **3** (PXRD simulated from single crystal data) visualized under UV (320 nm) light.

Table 3 Quantum yields of L and **1–3** in the solid state and in cellulose, polymethylmethacrylate (PMMA), polystyrene (PS) and Zeonex matrixes

Compound	Φ_{fl} (solid)	Φ_{fl} (cellulose)	Φ_{fl} (PMMA)	Φ_{fl} (PS)	Φ_{fl} (Zeonex)
L	0.36	0.91	0.96	0.95	0.93
1	0.01	0.12	0.13	0.13	0.31
2	0.03	0.87	0.90	0.93	0.83
3	0.03	0.56	0.57	0.58	0.53

Table 4 Lifetimes (ns) of L and **1–3** in the solid state and in cellulose, polymethylmethacrylate (PMMA), polystyrene (PS) and Zeonex matrixes

Compound	τ_{fl} (solid)	τ_{fl} (cellulose)	τ_{fl} (PMMA)	τ_{fl} (PS)	τ_{fl} (Zeonex)
L	5.80	9.69	9.07	8.01	8.4
1	4.08	6.93	7.02	6.49	7.43
2	3.59	8.02	8.22	6.93	6.74
3	4.18	6.93	5.62	5.31	5.59

Table 5 Radiative and non-radiative constants (ns^{-1}) of L and 1–3 in the solid state and in matrixes of cellulose, poly methyl methacrylate (PMMA), polystyrene (PS) and Zeonex

	Solid		Cellulose		PMMA		PS		Zeonex	
Compound	k_r	k_{nr}	k_r	k_{nr}	k_r	k_{nr}	k_r	k_{nr}	k_r	k_{nr}
L	0.062	0.11	0.094	0.009	0.11	0.004	0.12	0.006	0.11	0.008
1	0.0024	0.24	0.017	0.13	0.018	0.012	0.02	0.13	0.042	0.093
2	0.0072	0.27	0.10	0.016	0.11	0.012	0.13	0.010	0.12	0.025
3	0.007	0.23	0.08	0.063	0.10	0.076	0.11	0.079	0.09	0.084

comparable values to the rest of the gold(I) complexes in this medium. The quantum yield variation of **2** in the matrixes in comparison with the solid state should be highlighted since it goes from almost non-emissive powder to near unity efficiency.

Conclusions

Three new luminescent gold(I) complexes have been synthesized by combining an ethynyl-functionalized 2,1,3-benzothiadiazole (BTD), with different N-heterocyclic (imidazole, benzimidazole and phenantroimidazole) carbene gold(I) complexes. The BTD ligand is endowed with a terminal phenylnonyl moiety to induce the assembly of these molecules into layers. We have found that the nature of the N-heterocyclic carbene affects the relative disposition conformation of the two ligands in the linear gold complexes and subsequently the intermolecular interactions in the solid. Particularly the incorporation of a phenantroimidazole carbene with a larger extended π-system gives rise to a planar conformation which allowed gold atoms to get sufficiently closer to establish Au(I) ···Au(I) interactions. This compound can be obtained as different colour light emitting polymorphs probably reflecting the different strength of their aurophilic interactions.

The incorporation of the compounds in polymer matrixes enhanced the emissive properties of the compounds allowing the possibility of the incorporation of these compounds in devices to produce highly luminescent materials. This is of great advantage to produce luminescent materials with near unity quantum yields while the emission in the solid state is almost quenched.

Experimental section

General procedures

All manipulations have been performed under pre-purified N_2 using standard Schlenk techniques. All solvents have been distilled from appropriated drying agents. Commercial reagents imidazole (Aldrich >99.5%), iodoethane (Aldrich, 99%), 1*H*-benzo[*d*]imidazole (Fluorochem), 9,10-phenanthrenequinone (Fluorochem), and silver(I) oxide (Alfa Aesar, 99%) were used as received. Literature methods have been used to prepare 4-ethynyl-7-(4-nonylphenyl)benzo[*c*][1,2,5]thiadiazole (**L**).[47]

Physical measurements

Infrared spectra have been recorded on a FT-IR 520 Nicolet Spectrophotometer. ^{1}H-NMR (δ(TMS) = 0.0 ppm) spectra have been recorded on a Varian Mercury 400 and Bruker 400 (Universitat de Barcelona). ElectroSpray-Mass spectra (+) have been recorded on a Fisons VG Quatro spectrometer (Universitat de Barcelona). Absorption spectra have been recorded on a Varian Cary 100 Bio UV-spectrophotometer and emission spectra on a Horiba-Jobin-Ybon SPEX Nanolog spectrofluorimeter (Universitat de Barcelona). Luminescence quantum yields were recorded using an Absolute PL quantum yield spectrometer from Hamamatsu Photonics upon excitation of the samples at 400 nm. Fluorescence lifetimes were measured *via* the time-correlated single-photon counting technique (TCSPC) using DeltaPro fluorescence lifetime System from Horiba upon excitation of the sample with a 390 nm nanoLED. Crystals of **2** and **3** showing well defined faces were mounted on a Bruker Kappa Apex II (X8 APEX) diffractometer equipped with a Mo INCOATED microsource. Diffraction data were collected exploring over a hemisphere of reciprocal space in a combination of φ and ω scans to reach a resolution of 0.86 Å, using the Bruker APEXII software suite (APEX2; Bruker-AXS: Madison, WI, 2006). The structures were solved by the Multan and Fourier methods. Most of the calculations were carried out with APEXII software for data collection and reduction, and OLEX2 for structure solution and refinements. CCDC 2160186 and 2160187 contain the supplementary crystallographic data for this paper.†

Synthesis and characterization

Synthesis of *N*-ethyl-*N*′-ethylimidazolium iodide (Im1). Three steps are necessary for the synthesis of *N*-ethyl-*N*′-ethylimidazolium iodide. The first one is the deprotonation of the imidazole ring with a solution of sodium methoxide. Imidazole (0.290 g, 4.26 mmol) and small amount of acetonitrile (10 mL) were introduced into a solution of sodium methoxide (0.230 g, 4.25 mmol) in dry freshly distilled methanol at room temperature. After 15 min, a white suspension was formed and concentrated under reduced pressure. The dried white powder was dissolved in acetonitrile and iodoethane (2.030 g, 13.01 mmol) was added under a nitrogen atmosphere. The mixture was heated at 85 °C for 24 h. After the first alkylation, the same procedure was used for the second alkylation. After cooling to room temperature, the solvent was removed by evaporation under vacuum, and the brown solid obtained was exhaustively washed with pentane and dried. Yield: 70% (373 mg).

^{1}H NMR (CD_3OD, ppm): 1.55 (t, J = 4 Hz, 6H, N–CH_2–**CH_3** (ethyl)), 4.36 (q, J = 8 Hz, 4H, N–**CH_2**–CH_3 (ethyl)), 7.80 (s, 2H, CH–**CH**–N (imidazole)), 9.27 (s, 1H, N–**CH**–N (imidazole)). IR (KBr, cm^{-1}): ν(═CH–): 3075, ν(N═C): 1560. MALDI-TOF (+) m/z: 125.1 (M^+, calc.: 125.1).

Synthesis of 1,3-diethyl-1*H*-benzo[*d*]imidazol-3-ium iodide (Im2). Three steps are necessary for the synthesis of 1,3-diethyl-1*H*-benzo[*d*]imidazol-3-ium iodide. The first one is the deprotonation of the imidazole ring with a solution of sodium methoxide. 1*H*-Benzo[*d*]imidazole (0.300 g, 2.54 mmol) and a small amount of acetonitrile (10 mL) were introduced into a solution of sodium methoxide (0.139 g, 2.57 mmol) in dry freshly distilled methanol at room temperature. After 15 min of stirring a white suspension was formed and concentrated under reduced pressure. The dried white powder was dissolved in acetonitrile and iodoethane (613 μL, 7.62 mmol) was added under a nitrogen atmosphere. The mixture was heated at 85 °C for 24 h. After the first alkylation, the same procedure was used for the second alkylation. After cooling to room temperature, the solvent was removed by evaporation under vacuum, and the brown solid obtained was washed repeatedly with pentane and dried. Yield: 80% (356 mg).

^{1}H NMR (DMSO-d_6, ppm): 1.54 (t, J = 7.2 Hz, 6H, N–CH_2–**CH_3** (ethyl)), 4.51 (q, J = 7.2 Hz, 4H, N–**CH_2**–CH_3 (ethyl)), 7.69 (dd, J = 9.6 Hz, J = 3.2 Hz, 2H, C–CH–CH (benzo[*d*]imidazole)), 8.07 (dd, J = 9.6 Hz, J = 3.2 Hz, 2H, C–CH–CH (benzo[*d*]imidazole)), 9.74 (s, 1H, N–**CH**–N (benzo[*d*]imidazole)) IR (KBr, cm^{-1}): ν(═CH–): 3080, ν(N═C): 1555. ESI (+) m/z: 175.1217 (M^+, calc.:175.1230).

Synthesis of 1*H*-phenanthro[9,10-*d*]imidazole. A mixture of 9,10-phenanthrenequinone (0.200 g, 0.96 mmol), formaldehyde (0.214 mL, 2.88 mmol), glacial acetic acid (5 mL) and ammonium acetate (1.550 g, 20.16 mmol) was refluxed for 4 h. After cooling at room temperature, the reaction mixture was diluted with water and neutralized with concentrated aqueous ammonia until pH 7. A light cream precipitate was formed. It was filtered, washed with water, acetone, dichloromethane, and ethyl ether and then dried. Yield: 98% (206 mg).

^{1}H NMR (DMSO-d_6, ppm): 7.48 (t, J = 7.2 Hz, 2H, H_{phen}), 7.59 (t, J = 7.2 Hz, 2H, H_{phen}), 8.01 (s, 1H, N–CH–NH), 8.42 (d, J = 8 Hz, 2H, H_{phen}), 8.75 (d, J = 8 Hz, 2H, H_{phen}), 13.38 (br. s, 1H, N–H). IR (KBr, cm^{-1}): ν(═CH–): 3070, ν(N═C): 1565. ESI (+) m/z: 219.09 ($[M + H]^+$, calc.: 219.08).

Synthesis of 1,3-diethyl-1*H*-phenanthro[9,10-*d*]imidazol-3-ium iodide (Im3). Three steps are necessary for the synthesis of 1,3-diethyl-1*H*-phenanthro[9,10-*d*]imidazol-3-ium iodide. The first one is the deprotonation of the imidazole ring. To a solution of 1*H*-phenanthro[9,10-*d*]imidazole (0.300 g, 1.37 mmol) in acetonitrile (5 mL) and DMSO (2 mL) was added sodium hydroxide (0.055 g, 1.38 mmol). The reaction mixture was stirred at room temperature for 2.5 h. The temperature was increased to 37 °C, and the reaction mixture was stirred at this temperature overnight. The solvent was removed until an oil was formed and a precipitate was generated using diethyl ether. The dried solid was dissolved in DMF (5 mL) and iodoethane (332 μL, 4.11 mmol) was added. The mixture was heated at 130 °C during 24 h. After the first alkylation, the same procedure was used for the second alkylation. After cooling up to room temperature, water was added, and a red precipitate was formed. It was filtered, washed with water and ethyl ether and then dried. Yield: 50% (188 mg).

^{1}H NMR (DMSO-d_6, ppm): 1.68 (t, J = 7.2 Hz, 6H, N–CH_2–**CH_3** (ethyl)), 4.98 (q, J = 7.2 Hz, 4H, N–**CH_2**–CH_3 (ethyl)), 7.92 (m, 4H, H_{phen}), 8.61 (d, J = 8.4 Hz, 2H, H_{phen}), 9.12 (d, J = 8.4 Hz, 2H, H_{phen}), 9.74 (s, 1H, N–CH–N). ^{13}C NMR (DMSO-d_6, ppm): 141.54, 140.87, 129.81, 129.24, 128.98, 128.58, 126.30, 125.27, 122.94, 120.98, 46.25, 15.06. IR (KBr, cm^{-1}): ν(═CH–): 3070, ν(N═C): 1565. ESI (+) m/z: 275.1563 (M^+, calc.: 275.1543).

Synthesis of (*N*-ethyl-*N*′-ethylimidazolium)gold(I) chloride

Silver(I) oxide (0.0459 g, 0.19 mmol) was added to a solution of *N*-ethyl-*N*′-ethylimidazolium iodide (0.100 g, 0.33 mmol) in degassed dichloromethane (20 mL). The mixture was stirred under nitrogen for 6 h at 40 °C. [AuCl(tht)] (0.130 g, 0.33 mmol) was added after the mixture was cooled to room temperature and the mixture was stirred overnight. The solution was filtered through Celite and concentrated in a vacuum to half volume and hexane (10 mL) was then added in order to favour precipitation. The resulting orange solid was filtered and dried under vacuum. Yield: 70% (47 mg).

^{1}H NMR (CD_3OD, ppm): 1.46 (t, J = 7.2 Hz, 6H, N–CH_2–**CH_3** (ethyl)), 4.21 (q, J = 7.6 Hz, 4H, N–**CH_2**–CH_3 (ethyl)), 7.29 (s, 2H, CH–**CH**–N (imidazole)). ^{13}C NMR ($CDCl_3$, ppm): 169.88, 119.87, 46.55, 16.51. IR (KBr, cm^{-1}): ν(═CH–): 3090, ν(N═C): 1565. ESI (+) m/z: 348.077 ($[M - Cl + CN + H]^+$, calc.: 348.069).

Synthesis of (1,3-diethyl-1*H*-benzo[*d*]imidazol-3-ium)gold(I) chloride. Silver(I) oxide (0.038 g, 0.16 mmol) was added to a solution of 1,3-diethyl-1*H*-benzo[*d*]imidazol-3-ium iodide (0.1 g, 0.33 mmol) in degassed dichloromethane (20 mL). The mixture was stirred under nitrogen for 6 h at 40 °C. After the mixture was cooled to room temperature, [AuCl(tht)] (0.106 g, 0.33 mmol) was added and the mixture was stirred overnight at room temperature. The solution was filtered through Celite and concentrated in vacuum to half volume and hexane (10 mL) was added in order to favour precipitation. The resulting orange solid was filtered and dried under vacuum. Yield: 75% (49 mg).

^{1}H NMR ($CDCl_3$, ppm): 1.54 (t, J = 7.6 Hz, 6H, N–CH_2–**CH_3** (ethyl)), 4.54 (q, J = 7.2 Hz, 4H, N–**CH_2**–CH_3 (ethyl)), 7.43 (dd, J = 9.2 Hz, J = 3.2 Hz, 2H, C–CH–CH (benzo[*d*]imidazole)), 7.49 (dd, J = 9.2 Hz, J = 3.2 Hz, 2H, C–CH–CH (benzo[*d*]imidazole)). IR (KBr, cm^{-1}): ν(═CH–): 3080, ν(N═C): 1555. ESI (+) m/z: 398.093 ($[M - Cl + CN + H]^+$, calc.: 398.085).

Synthesis of (1,3-diethyl-1*H*-phenanthro[9,10-*d*]imidazol-3-ium)gold(I) chloride. 1,3-Diethyl-1*H*-phenanthro[9,10-*d*]imidazol-3-ium iodide (0.075 g, 0.19 mmol) was mixed with Ag_2O (0.043 g, 0.18 mmol), 3 Å molecular sieves (0.1 g) and dry CH_2Cl_2 (5 mL) and stirred at 40 °C for 72 h. Then, [AuCl(tht)] (0.059 g, 0.19 mmol) was added and the mixture was stirred overnight at room temperature. The solution was filtered through Celite and concentrated in a vacuum to half volume

and hexane (5 mL) was added in order to favor precipitation. The resulting red solid was filtered and dried under vacuum. Yield: 45% (50 mg).

^{1}H NMR (DMSO-d_6, ppm): 1.38 (t, J = 7.08 Hz, 6H, N–CH_2–**CH_3** (ethyl)), 4.46 (q, J = 7.12 Hz, 4H, N–**CH_2**–CH_3 (ethyl)), 7.64 (t, J = 7.8 Hz, 2H, H_{phen}), 7.75 (t, J = 7.32, 2H, H_{phen}), 8.37 (d, J = 8.4 Hz, 2H, H_{phen}), 8.97 (d, J = 8.4 Hz, 2H, H_{phen}). ^{13}C NMR (DMSO-d_6, ppm): 129.29, 128.93, 127.46, 126.65, 125.12, 122.51, 121.21, 117.34, 47.55, 16.11. IR (KBr, cm^{-1}): ν(═CH–): 3070, ν(N═C): 1565. ESI (+) m/z: 498.124 ([M − Cl + CN + H]$^+$, calc.: 498.117).

Synthesis of [Au(4-ethynyl-7-(4-nonylphenyl)benzo[*c*][1,2,5]thiadiazole) (*N*-ethyl-*N*′-ethylimidazolium)] (1). To a stirred solution of 4-ethynyl-7-(4-nonylphenyl)benzo[*c*][1,2,5]thiadiazole (0.051 g, 0.14 mmol) in THF–MeOH (2 : 1, v/v, 25 mL) was added KOH (0.019 g, 0.34 mmol). The reaction was stirred under nitrogen for 15 min. To the stirred yellow solution was added (*N*-ethyl-*N*′-ethylimidazolium)gold(I) chloride (0.050 g, 0.14 mmol). The solution was stirred overnight under nitrogen. The mixture was concentrated in a vacuum to half volume and hexane (10 mL) was added in order to favour precipitation. The resulting yellow solid was filtered and dried under vacuum. Yield: 60% (57 mg).

^{1}H NMR (CD_3OD, ppm): 0.90 (t, J = 7.2 Hz, 3H), 1.30–1.37 (m, 21H), 1.50 (t, J = 7.2 Hz, 6H, N–CH_2–**CH_3** (ethyl)), 1.68 (m, 2H), 2.70 (t, J = 7.6 Hz, 2H), 4.28 (q, J = 7.2 Hz, 4H, N–**CH_2**–CH_3 (ethyl)), 7.29 (s, 2H, CH–**CH**–N (imidazole)), 7.32 (d, J = 8 Hz, 2H), 7.72 (d, J = 5.6 Hz, 2H), 7.90 (d, J = 8 Hz, 2H). ^{13}C NMR ($CDCl_3$, ppm): 156.69, 153.49, 144.59, 142.93, 135.06, 132.10, 130.97, 128.96, 128.82, 128.64, 128.10, 120.59, 120.15, 119.87, 99.66, 46.60, 35.80, 21.92, 31.47, 29.57, 29.36, 22.70, 16.86, 14.14. IR (KBr, cm^{-1}): ν(═CH–): 3090, ν(C≡C): 2108, ν(N═C): 1565. ESI (+) m/z: 683.248 ([M + H]$^+$, calc.: 683.240).

Synthesis of [Au(4-ethynyl-7-(4-nonylphenyl)benzo[*c*][1,2,5]thiadiazole) (1,3-diethyl-1*H*-benzo[*d*]imidazol-3-ium)] (2). To a stirred solution of 4-ethynyl-7-(4-nonylphenyl)benzo[*c*][1,2,5]thiadiazole (0.044 g, 0.12 mmol) in THF–MeOH (2 : 1, v/v, 25 mL) was added KOH (0.017 g, 0.31 mmol). The reaction was stirred under nitrogen for 15 min. To the stirred yellow solution was added (1,3-diethyl-1*H*-benzo[*d*]imidazol-3-ium iodide) gold(I) chloride (0.050 g, 0.12 mmol). The solution was stirred overnight under nitrogen. The mixture was concentrated in a vacuum to half volume and hexane (10 mL) was added in order to favour precipitation. The resulting yellow solid was filtered and dried under vacuum. Yield: 70% (61 mg).

^{1}H NMR ($CDCl_3$, ppm): 0.88 (t, J = 6.8 Hz, 3H), 1.27–1.35 (m, 21H), 1.66 (m, 2H), 2.68 (t, J = 8 Hz, 2H), 4.61 (q, J = 7.6 Hz, 4H, N–**CH_2**–CH_3 (ethyl)), 7.33 (d, J = 8.4 Hz, 2H), 7.42 (dd, J = 9.2 Hz, J = 2.8 Hz, 2H, C–CH–CH (benzo[*d*]imidazole)), 7.49 (dd, J = 9.2 Hz, J = 2.8 Hz, 2H, C–CH–CH (benzo[*d*]imidazole)), 7.62 (d, J = 7.6 Hz, 1H), 7.82 (d, J = 7.2 Hz, 1H), 7.86 (d, J = 8 Hz, 2H). ^{13}C NMR ($CDCl_3$, ppm): 193.03, 156.48, 153.21, 143.20, 138.52, 134.83, 133.12, 132.53, 128.98, 128.67, 127.75, 124.16, 118.05, 111.30, 100.69, 43.62, 35.82, 31.92, 29.57, 29.41, 29.36, 22.70, 15.72, 14.14. IR (KBr, cm^{-1}): ν(═CH–):3080, ν(C≡C): 2110 ν(N═C): 1555. ESI (+) m/z: 733.262 ([M + H]$^+$, calc.: 733.256).

Synthesis of [Au(4-ethynyl-7-(4-nonylphenyl)benzo[*c*][1,2,5]thiadiazole) (1,3-diethyl-1*H*-phenanthro[9,10-*d*]imidazol-3-ium)] (3). To a stirred solution of 4-ethynyl-7-(4-nonylphenyl)benzo[*c*][1,2,5]thiadiazole (0.014 g, 0.039 mmol) in THF–MeOH (2 : 1, v/v, 25 mL) was added KOH (0.005 g, 0.096 mmol). The reaction was stirred under nitrogen for 15 min. To the stirred yellow solution was added (1,3-diethyl-1*H*-phenanthro[9,10-*d*]imidazol-3-ium)gold(I) chloride (0.020 g, 0.039 mmol). The solution was stirred overnight under nitrogen. The mixture was concentrated in a vacuum to half volume and hexane (10 mL) was added in order to favour precipitation. The resulting yellow solid was filtered and dried under vacuum. Yield: 50% (6 mg).

^{1}H NMR ($CDCl_3$, ppm):0.88 (t, J = 6.2 Hz, 3H), 1.26–1.40 (m, 21H), 1.68 (t, J = 8.3 Hz, 2H), 1.74 (t, J = 7.2 Hz, 6H, N–CH_2–**CH_3** (ethyl)), 2.68 (t, J = 7.7 Hz, 2H), 5.22 (q, J = 7.2 Hz, 4H, N–**CH_2**–CH_3 (ethyl)), 7.34 (d, J = 8.1 Hz, 2H), 7.63 (d, J = 7.3 Hz, 1H), 7.76 (t, J = 8.3 Hz, 4H, H_{phen}), 7.84 (d, J = 7.4 Hz, 1H), 7.88 (d, J = 8.1 Hz, 2H), 8.41 (d, J = 8.2 Hz, 2H, H_{phen}), 8.86 (d, J = 8.2 Hz, 2H, H_{phen}). ^{13}C NMR ($CDCl_3$, ppm): 155.47, 152.20, 142.17, 131.51, 128.35, 127.96, 127.65, 126.99, 126.75, 125.94, 125.53, 120.55, 117.09, 45.97, 39.62, 34.78, 33.72, 30.88, 30.42, 28.54, 28.33, 21.66, 15.12, 13.09. IR (KBr, cm^{-1}): ν(═CH–): 3070, ν(C≡C): 2110, ν(N═C): 1565. ESI (+) m/z: 833.327 ([M + H]$^+$, calc.: 833.287).

Preparation of matrixes doped with L and 1–3 complexes

Cellulose, PMMA, PS and Zeonex (Zeon Corporation, Japan) were used as matrix polymers. The films were prepared *via* drop-casting, using a mixture of the dopant and the host (Cellulose, PMMA, PS or Zeonex). Polymer solutions were prepared as follows: PMMA (MW 120 000, 30% solution in dichloromethane), PS (MW 45 000, 35% solution in dichloromethane), cellulose (MW 30 000, 20% in acetone), and Zeonex (20% in chloroform). To a polymer solution was added the same volume of a solution of the sample at a concentration of 20 μg mL^{-1}. The films were drop-cast onto a quartz substrate at room temperature to avoid any thermal annealing.

Conflicts of interest

There are no conflicts of interest to declare.

Acknowledgements

The authors are grateful to Projects PID2019-104121GB-I00 and PID2019-104125RB-I00 funded by the Ministerio de Ciencia e Innovación of Spain MCIN/AEI/10.13039/501100011033. We gratefully acknowledge Dr Josefina Perles for solving the crystal structure of **2** and **3**. We are indebted to Zeon Europe GmbH for providing us with Zeonex 480.

References

1 S. N. Islam, A. Sil and S. K. Patra, *Dalton Trans.*, 2017, **46**, 5918–5929.
2 L. J. Xu, X. Zhang, J. Y. Wang and Z. N. Chen, *J. Mater. Chem. C*, 2016, **4**, 1787–1794.
3 C. Fan and C. Yang, *Chem. Soc. Rev.*, 2014, **43**, 6439–6469.
4 C.-L. Ho, Z.-Q. Yu and W.-Y. Wong, *Chem. Soc. Rev.*, 2016, **45**, 5264–5295.
5 G. R. Whittell, M. D. Hager, U. S. Schubert and I. Manners, *Nat. Mater.*, 2011, **10**, 176–188.
6 X. Yang, G. Zhou and W. Y. Wong, *Chem. Soc. Rev.*, 2015, **44**, 8484–8575.
7 N. Sun, C. Jiang, Q. Li, D. Tan, S. Bi and J. Song, *J. Mater. Sci.: Mater. Electron.*, 2020, **31**, 20688–20729.
8 Y. Xu, P. Xu, D. Hu and Y. Ma, *Chem. Soc. Rev.*, 2021, **50**, 1030–1069.
9 S. Varughese, *J. Mater. Chem. C*, 2014, **2**, 3499–3516.
10 M. Echeverri, I. Martín, A. Concellón, C. Ruiz, M. S. Anselmo, E. Gutiérrez-Puebla, J. L. Serrano and B. Gómez-Lor, *ACS Omega*, 2018, **3**, 11857–11864.
11 S. I. Stupp and L. C. Palmer, *Chem. Mater.*, 2014, **26**, 507–518.
12 V. H. K. Fell, N. J. Findlay, B. Breig, C. Forbes, A. R. Inigo, J. Cameron, A. L. Kanibolotsky and P. J. Skabara, *J. Mater. Chem. C*, 2019, **7**, 3934–3944.
13 J. Yuan, Y. Zhang, L. Zhou, C. Zhang, T. K. Lau, G. Zhang, X. Lu, H. L. Yip, S. K. So, S. Beaupré, M. Mainville, P. A. Johnson, M. Leclerc, H. Chen, H. Peng, Y. Li and Y. Zou, *Adv. Mater.*, 2019, **31**, 1–8.
14 B. A. D. Neto, P. H. P. R. Carvalho and J. R. Correa, *Acc. Chem. Res.*, 2015, **48**, 1560–1569.
15 W.-Q. Zhang, K. Cheng, X. Yang, Q.-Y. Li, H. Zhang, Z. Ma, H. Lu, H. Wu and X.-J. Wang, *Org. Chem. Front.*, 2017, **4**, 1719–1725.
16 M. Echeverri, C. Ruiz, S. Gámez-Valenzuela, M. Alonso-Navarro, E. Serrano, J. L. Gutierrez-Puebla, M. C. Ruiz Delgado and B. Gómez-Lor, *ACS Appl. Mater. Interfaces*, 2020, **12**, 10929–10937.
17 B. Gómez-Lor, L. M. Aguirre-Díaz, M. Echeverri, C. Ruiz, S. Gámez-Valenzuela, I. Martín, M. C. R. Delgado, E. Gutiérrez-Puebla and M. Á. Monge, *J. Am. Chem. Soc.*, 2020, **142**, 17147–17155.
18 V. S. Souza, J. R. Corrêa, P. H. P. R. Carvalho, G. M. Zanotto, G. I. Matiello, B. C. Guido, C. C. Gatto, G. Ebeling, P. F. B. Gonçalves, J. Dupont and B. A. D. Neto, *Sens. Actuators, B*, 2020, **321**, 128530.
19 J. C. Lima and L. Rodríguez, *Inorganics*, 2015, **3**, 1–18.
20 E. Aguiló, R. Gavara, C. Baucells, M. Guitart, J. C. Lima, J. Llorca and L. Rodríguez, *Dalton Trans.*, 2016, **45**, 7328–7339.
21 A. Pinto, N. Svahn, J. C. Lima and L. Rodríguez, *Dalton Trans.*, 2017, **46**, 11125–11139.
22 E. Aguiló, A. J. Moro, R. Gavara, I. Alfonso, Y. Pérez, F. Zaccaria, C. F. Guerra, M. Malfois, C. Baucells, M. Ferrer, J. C. Lima and L. Rodríguez, *Inorg. Chem.*, 2018, **57**, 1017–1028.
23 A. Pinto, G. Hernández, R. Gavara, E. Aguiló, A. J. Moro, G. Aullón, M. Malfois, J. C. Lima and L. Rodríguez, *New J. Chem.*, 2019, **43**, 8279–8289.
24 A. Pinto, C. Roma-Rodrigues, J. S. Ward, R. Puttreddy, K. Rissanen, P. V. Baptista, A. R. Fernandes, J. C. Lima and L. Rodríguez, *Inorg. Chem.*, 2021, **60**, 18753–18763.
25 H. Ito, T. Saito, N. Oshima, N. Kitamura, S. Ishizaka and Y. Hinatsu, *J. Am. Chem. Soc.*, 2008, **2**, 10044–10045.
26 Q. Liu, M. Xie, X. Chang, Q. Gao, Y. Chen and W. Lu, *Chem. Commun.*, 2018, **54**, 12844–12847.
27 M. Osawa, I. Kawata, S. Igawa, M. Hoshino, T. Fukunaga and D. Hashizume, *Chem. – Eur. J.*, 2010, **16**, 12114–12126.
28 M. Echeverri, C. Ruiz and B. Gómez-Lor, *CrystEngComm*, 2021, **23**, 5925–5930.
29 S. Livi, J. F. Gérard and J. Duchet-Rumeau, *Chem. Commun.*, 2011, **47**, 3589–3591.
30 J. Arcau, V. Andermark, M. Rodrigues, I. Giannicchi, L. Pérez-Garcia, I. Ott and L. Rodríguez, *Eur. J. Inorg. Chem.*, 2014, 6117–6125.
31 D. Tapu, C. Owens, D. Vanderveer and K. Gwaltney, *Organometallics*, 2009, **6**, 270–276.
32 R. Rubbiani, I. Kitanovic, H. Alborzinia, S. Can, A. Kitanovic, L. A. Onambele, M. Stefanopoulou, Y. Geldmacher, W. S. Sheldrick, G. Wolber, A. Prokop, S. Wölfl and I. Ott, *J. Med. Chem.*, 2010, **53**, 8608–8618.
33 S. Ibáñez, M. Poyatos and E. Peris, *J. Organomet. Chem.*, 2020, **917**, 121284.
34 S. M. Meier-Menches, B. Aikman, D. Döllerer, W. T. Klooster, S. J. Coles, N. Santi, L. Luk, A. Casini and R. Bonsignore, *J. Inorg. Biochem.*, 2020, **202**, 110844.
35 M. R. Ams, N. Trapp, A. Schwab, J. V. Milić and F. Diederich, *Chem. – Eur. J.*, 2019, **25**, 323–333.
36 I. Tanabe, Y. Kurawaki, Y. Morisawa and Y. Ozaki, *Phys. Chem. Chem. Phys.*, 2016, **18**, 22526–22530.
37 A. Pazini, L. Maqueira, F. da Silveira Santos, A. R. Jardim Barreto, R. dos S. Carvalho, F. M. Valente, D. Back, R. Q. Aucélio, M. Cremona, F. S. Rodembusch and J. Limberger, *Dyes Pigm.*, 2020, **178**, 108377.
38 S. Goswami, R. W. Winkel and K. S. Schanze, *Inorg. Chem.*, 2015, **54**, 10007–10014.
39 P. Gautam, R. Maragani, S. M. Mobin and R. Misra, *RSC Adv.*, 2014, **4**, 52526–52529.
40 S. Goswami, G. Wicks, A. Rebane and K. S. Schanze, *Dalton Trans.*, 2014, **43**, 17721–17728.
41 C. S. Abeywickrama, K. J. Wiesinghe, R. V. Stahelin and Y. Pang, *Sens. Actuators, B*, 2019, **285**, 76–83.
42 A. Möller, P. Bleckenwegner, U. Monkowius and F. Mohr, *J. Organomet. Chem.*, 2016, **813**, 1–6.
43 P. Rietsch, S. Sobottka, K. Hoffmann, A. A. Popov, P. Hildebrandt, B. Sarkar, U. Resch-Genger and S. Eigler, *Chem. – Eur. J.*, 2020, **26**, 17361–17365.
44 P. Rietsch, S. Sobottka, K. Hoffmann, P. Hildebrandt, B. Sarkar, U. Resch-Genger and S. Eigler, *ChemPhotoChem*, 2020, **4**, 668–673.

45 J. Pina, J. S. De Melo, D. Breusov and U. Scherf, *Phys. Chem. Chem. Phys.*, 2013, **15**, 15204–15213.
46 J. Zhang, A. Konsmo, A. Sandberg, X. Wu, S. Nyström, U. Obermüller, B. M. Wegenast-Braun, P. Konradsson, M. Lindgren and P. Hammarström, *J. Med. Chem.*, 2019, **62**, 2038–2048.
47 A. Pinto, M. Echeverri, B. Gómez-Lor and L. Rodríguez, *Dyes Pigm.*, 2022, DOI: **10.1016/j.dyepig.2022.110308**.